AAC Journals.ASM.org

In Vivo Monitoring of *Staphylococcus aureus* Biofilm Infections and Antimicrobial Therapy by [^{18}F]Fluoro-Deoxyglucose–MicroPET in a Mouse Model

Victoria Garrido,[a] María Collantes,[b] Montserrat Barberán,[c] Iván Peñuelas,[b,d] Javier Arbizu,[d] Beatriz Amorena,[a] María-Jesús Grilló[a]

Grupo de Sanidad Animal, Instituto de Agrobiotecnología (CSIC-UPNA-Gobierno de Navarra), Mutilva, Navarra, Spain[a]; Unidad de Investigación MicroPET, Center for Applied Medical Research (CIMA) and Clínica Universidad de Navarra, Pamplona, Spain[b]; Unidad de Histología y Anatomía Patológica, Facultad de Veterinaria, Universidad de Zaragoza, Zaragoza, Spain[c]; Servicio de Medicina Nuclear, Clínica Universidad de Navarra, Pamplona, Spain[d]

A mouse model was developed for *in vivo* monitoring of infection and the effect of antimicrobial treatment against *Staphylococcus aureus* biofilms, using the [^{18}F]fluoro-deoxyglucose–MicroPET ([^{18}F]FDG-MicroPET) image technique. In the model, sealed Vialon catheters were briefly precolonized with *S. aureus* strains ATCC 15981 or V329, which differ in cytotoxic properties and biofilm matrix composition. After subcutaneous implantation of catheters in mice, the *S. aureus* strain differences found in bacterial counts and the inflammatory reaction triggered were detected by the regular bacteriological and histological procedures and also by [^{18}F]FDG-MicroPET image signal intensity determinations in the infection area and regional lymph node. Moreover, [^{18}F]FDG-MicroPET imaging allowed the monitoring of the rifampin treatment effect, identifying the periods of controlled infection and those of reactivated infection due to the appearance of bacteria naturally resistant to rifampin. Overall, the mouse model developed may be useful for noninvasive *in vivo* determinations in studies on *S. aureus* biofilm infections and assessment of new therapeutic approaches.

Often, *in vivo* bacterial biofilms are inadvertently undetected since viable bacteria are shed only periodically. This hampers diagnosis, which often requires puncture biopsy and/or surgery, with the associated cost, morbidity, and mortality. *Staphylococcus aureus* is one of the most frequent device-associated pathogens. In staphylococcal biofilms, bacterial cells are interconnected by different types of polymeric matrices, including, among others, those composed of polysaccharide intercellular adhesin (PIA), also known as [polymeric *N*-acetyl-β-(1,6)-glucosamine] (PNAG), or proteins such as Bap (1–7). Of these, PIA/PNAG matrices are particularly common in clinical isolates (2) and medical device-related biofilm infections by *S. aureus* (mainly methicillin-susceptible *S. aureus* [MSSA]) and *Staphylococcus epidermidis* (8, 9).

Subcutaneous catheters have been successfully used in models that simulate natural device-related staphylococcal infections. However, with the use of nonsealed catheters in these models, the biofilm may be developed inside the catheter lumen, allowing only a partial interaction between bacteria and the immune system cells (10, 11).

Although *S. aureus* biofilm infections have been widely characterized and quantified, especially *in vitro*, an experimental noninvasive model to assess biofilm infections by natural or genetically modified bacteria is still needed to monitor *in vivo* infection and treatment efficacy in preclinical studies. One of the most useful animal models developed so far requires the use of bioluminescent *S. aureus* bacteria genetically modified to contain *lux* genes (12, 13). The use of this method is particularly limited when infections are caused by nonbioluminescent bacteria or in long-term studies, in which loss of bioluminescence may occur (14).

Positron emission tomography (PET) with [^{18}F]fluoro-deoxyglucose ([^{18}F]FDG), an *in vivo* nuclear medicine imaging technique requiring the administration of this glucose analog radiotracer, is being successfully applied in clinical infections, since this radiotracer is metabolized by many infectious and inflammatory cells (15). This technique has been proposed for early detection of different infectious processes (16) and also in combination with magnetic resonance imaging for clinical and biomedical research (17). The main advantages of PET over other imaging techniques are its high sensitivity and the possibility to perform quantitative measurements in the images generated. In animals, [^{18}F]FDG-MicroPET has been used in different rabbit osteomyelitis models (18, 19). The most recent one was performed to detect staphylococcal infections in bone and compare *S. aureus* and *S. epidermidis* infections (18).

The aim of our study was to determine the utility of a noninvasive [^{18}F]FDG-MicroPET *in vivo* imaging technology, using a sealed-catheter mouse model, in order to assess *in vivo* infection differences between *S. aureus* biofilm-producing strains and to monitor as well the effect of antimicrobial treatment in longitudinal studies. Results regarding strain virulence, inflammatory responses, and the [^{18}F]FDG-MicroPET signal were investigated.

MATERIALS AND METHODS

Bacterial strains and culture conditions. Two *S. aureus* wild-type strains (ATCC 15981 and V329) having a high capacity to form biofilms but triggering different types of infections (clinical and subclinical, respectively) were used. Strain ATCC 15981 was from a human clinical otitis patient. This *bap*-negative strain contained genes encoding exocellular proteases (20) and formed a highly adherent hyperbiofilm with an *ica*-dependent PIA/PNAG polysaccharidic matrix (21). Strain V329 was from

Received 21 April 2014 Returned for modification 26 May 2014
Accepted 16 August 2014
Published ahead of print 25 August 2014
Address correspondence to María Jesús Grilló, mariajesus.grillo@unavarra.es.

doi:10.1128/AAC.03138-14

bovine subclinical mastitis (1), produced a Bap protein biofilm matrix (21) expressed in a stable *ica*-independent manner *in vivo* (22), and had a very low pathogenicity in experimental animal infections (23). These strains were kindly provided by I. Lasa (Instituto de Agrobiotecnología, Pamplona, Spain) and J. Penadés (University of Glasgow, Glasgow, United Kingdom), respectively.

S. aureus bacteria were cultured (37°C, 18 h) in tryptone soy agar (TSA; Laboratorios Conda, Spain) or tryptone soy broth (TSB; Laboratorios Conda, Spain) supplemented with glucose (0.25%, wt/vol) (TSA-glc and TSB-glc, respectively). The bacterial concentration was first adjusted, spectrophotometrically and by dilution in TSB-glc, to 1×10^5 bacteria/ml for catheter infection. Exact doses (CFU/ml) were retrospectively assessed by serial 10-fold dilutions in phosphate buffer saline (PBS; pH 7.4), by plating (37°C, 18 h) 100 μl in triplicate (limit of detection, 3.3 CFU/ml) in TSA-glc, and incubation (37°C, 18 h).

Mouse model of *S. aureus* sealed-catheter infection. Female CD1 mice (Charles River International) of 20- to 22-g body weight were accommodated in the animal facilities of the Universidad Pública de Navarra (UPNA; registration code ES/31-2016-000002-CR-SU-US), with water and food *ad libitum*. Mouse handling and procedures were performed in compliance with the current European and national regulations, following the FELASA and ARRIVE welfare guidelines, and with the supervision of the UPNA's Comité de Ética, Experimentación Animal y Bioseguridad (CEEAB) and approval by the competent authority (Gobierno de Navarra).

To prepare implants, commercial Vialon 18G 1.3- by 30-mm catheters (Becton-Dickinson) were cut into 20-mm segments and sealed under sterile conditions with petrolatum and tissular glue (Vetbond; 3M España S.A.). Cleaning and disinfection were achieved thereafter by immersion in DD445 (A&B Laboratorios de Biotecnología) and ethanol (15 min in each solvent). Sterility was checked by incubation (37°C, 24 h) in TSB. Then, reliable *S. aureus* catheter precolonization was successfully achieved by incubation (37°C, 4 h) in 1 ml TSB-glc containing 1×10^5 CFU, as previously reported (10). The number of bacteria adhered to implants prior to infection was systematically assessed. Finally, catheters were rinsed with fresh TSB-glc and immediately implanted subcutaneously through a minimal surgical incision in the interscapular area of mice, previously anesthetized by intraperitoneal administration of ketamine (100 mg/kg of body weight; Imalgene; Merial Laboratorios, S.A.) and xylacine (10 mg kg^{-1}; Rompun; Bayer Health Care). In each experiment, nonprecolonized but TSB-glc-treated catheters were subcutaneously implanted in control mice.

Experimental design. Following implantation, four main animal experiments were carried out. A detailed description of each experiment is included below, and animal group distribution and assessment time points are summarized in Fig. 1.

Clinical and bacteriological studies. After catheter implantation in groups of 50 CD1 mice, animals were examined daily by palpation for the presence of catheter and signs of local infection through a 6-week period, and the number of bacteria adhered to the catheter was determined just before implantation (as baseline control) as well as at days 1, 2, 3, 4, and 7 and then weekly for 6 weeks postimplantation (PI) (Fig. 1A). For this, 5 mice per bacterial strain were euthanized by cervical dislocation and catheters were aseptically removed, homogenized in 1 ml PBS by ultrasound bath (40 to 50 Hz, 30 min; Selecta), and vortexed (1 min). The number of CFU per catheter was determined by serial 10-fold dilution of homogenates in PBS, plating 100 μl by triplicate in TSA, and incubation of plates (37°C, 18 to 24 h). Finally, the mean and standard deviation (SD) ($n = 5$) in $\log_{10}$ CFU/catheter were calculated.

Histopathological analysis and lesion score. Histological studies using hematoxylin and eosin (H&E) and immunohistochemical (IHC) staining were carried out in the subcutaneous tissue area surrounding the catheter implanted in mice, according to the scheme illustrated in Fig. 1B. For this, sealed catheters precolonized with *S. aureus* strain ATCC 15981 or V329 as described above were implanted subcutaneously in groups of

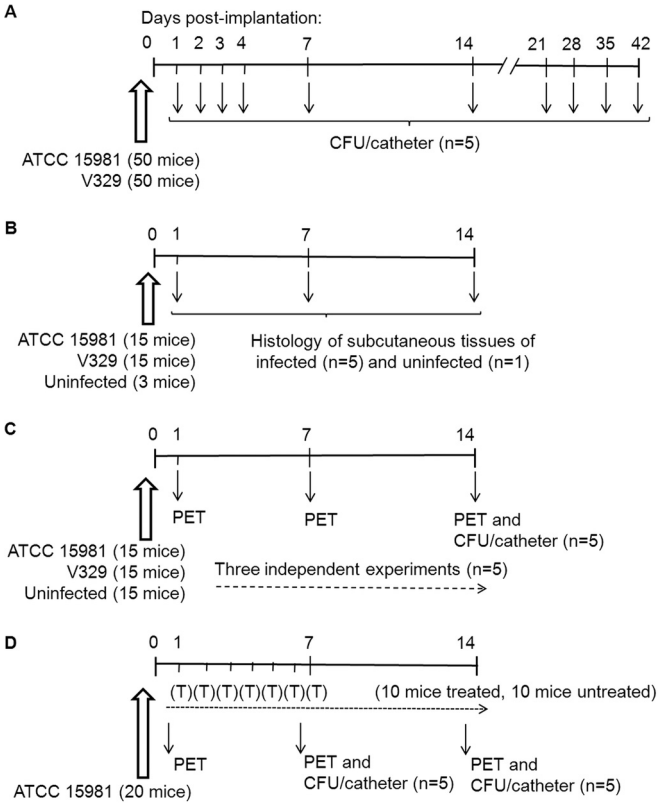

FIG 1 Design of the four mouse assays (A to D) performed in this work, according to animal group distribution and time points for analysis (indicated with arrows). (A) Bacteriological study on the evolution of infections ($\log_{10}$ CFU/catheter); (B) histological changes in subcutaneous tissue during infection, using hematoxylin and eosin (H&E) and immunohistochemical (IHC) staining; (C) *in vivo* [^{18}F]FDG-MicroPET imaging in an infection follow-up study; (D) [^{18}F]FDG-MicroPET imaging and bacteriological study ($\log_{10}$ CFU/catheter) in mice carrying infected catheters and then treated (T) daily for 1 week with rifampin (0.5 mg/day/mouse) or receiving PBS (untreated controls). Experiments illustrated in panels A, B, and C were carried out each independently with strains *S. aureus* ATCC 15981 and V329 and also included animal groups with uninfected catheters (control groups). The experiment shown in panel D was done with strain ATCC 15981.

15 CD1 mice, and tissue samples containing the catheter and surrounding tissues (adipose, muscular, and connective) were obtained at 1, 7, and 14 days PI ($n = 5$) and fixed for 24 h in 10% buffered formaldehyde solution. An additional group of 3 mice carrying sealed catheters preincubated in TSB-glc alone were used ($n = 1$) as uninfected controls. Five transaxial slices of tissues obtained every 2 to 3 mm were embedded in paraffin, and then, 4- to 6-μm sections were stained with H&E by standard procedures and examined for four histological features: (i) local inflammatory reaction by infiltration of polymorphonuclear leukocytes or mononuclear cells around the catheter; (ii) cellular debris and acellular exudates between the catheter and the inflammatory reaction; (iii) fibrosis and encapsulation of the reaction around the catheter; and (iv) diffuse inflammatory reaction located between the adipose, muscular, and other peripheral tissues. Lesions were scored on a scale of 0 to 4 (0, absent to very low; 1, mild; 2, moderate; 3, strong; 4, very strong).

Similar sections were stained for IHC studies to specifically detect the antigen PIA/PNAG (strain ATCC 15981) or Bap (strain V329). These sections were subjected to antigen retrieval by heating the slides in a pressure cooker for 3 min in distilled water, pH 4.0. The IHC staining was performed using polyclonal rabbit antibodies to PIA/PNAG and Bap, kindly provided by J. Pier (Harvard Medical School, USA) and J. Valle

(CSIC-Instituto de Agrobiotecnología, Spain), respectively. Primary antibodies were diluted 1:750 (PIA/PNAG) and 1:500 (Bap) with Dako antibody diluent (Dako Denmark A/S), and the reaction products were detected by using a Dako horseradish peroxidase (HRP) rabbit secondary antibody (Dako, Denmark A/S). Tissue preparations from mice carrying a noninfected sealed catheter were used as control. Additionally, conventional rabbit serum (product reference R9133; Sigma) was used as primary antibody control for the IHC technique specificity. Images were observed and digitalized using an Olympus Vanox AHBS3 microscope coupled to an Olympus DP12 digital camera.

Cytotoxicity assay. Cytotoxicity was measured by assessing the cytolytic effect of bacterial extracts, as described previously (24) but using the MDTF (*Mus dunni* tail fibroblast) murine cell line as targets. Briefly, bacterial extracts obtained from *S. aureus* strains ATCC 15981 or V329 were diluted (1:10, 1:100, and 1:1,000) in PBS and incubated (37°C, 5% CO_2) with 1×10^5 MDTF cells (reaching confluence)/well in 24-well plates (BD Biosciences) for 90 min. PBS-treated cell extracts were used as control. After incubation, cells were rinsed with PBS, detached with trypsin, centrifuged (1,000 × *g*, 5 min), and fixed with formalin. The number of live cells was determined by flow cytometry (FACS Scalibur, BD Biosciences).

[^{18}F]FDG-MicroPET *in vivo* monitoring of biofilm infections. Sealed catheters precolonized with either ATCC 15981 or V329 *S. aureus* strains were implanted subcutaneously in a total of 15 mice, as described above. An additional group of 15 mice carrying catheters pretreated with TSB-glc alone (see above) was used as uninfected control (Fig. 1C). Results were assessed in 3 independent experiments (5 mice per strain and experiment). Following catheter implantation, infection was longitudinally evaluated *in vivo* ($n = 5$) by [^{18}F]FDG-MicroPET on days 1, 7, and 14. For this, fasted mice were anesthetized with 2% isoflurane in O_2 gas and intravenously injected with 18.8 ± 1.9 MBq of [^{18}F]FDG. Following 1 h of radiotracer uptake under continuous anesthesia inhalation, PET imaging was performed in a small-animal tomograph (MicroPET; Mosaic; Philips, USA) by laying mice in prone position and capturing images for 15 min. Images were reconstructed using the three-dimensional (3D) Ramla algorithm (a true 3D reconstruction) with 2 iterations and a relaxation parameter of 0.024 into a 128 by 128 matrix with a 1-mm voxel size, applying dead time, decay, random, and scattering corrections.

For [^{18}F]FDG uptake assessment, MicroPET images were analyzed using the PMOD software (PMOD Technologies Ltd., Adliswil, Switzerland), and semiquantitative results were expressed as the standardized uptake value (SUV) index, obtained by normalization with the formula $SUV = [(RTA/cm^3)/RID] \times BW$, where RTA is the radiotracer tissue activity (in becquerels), RID is the radiotracer injected dose (in Bq), and BW is the mouse body weight (in grams). After qualitative inspection of the images, volumes of interest (VOI) were manually drawn on coronal 1-mm-thick consecutive slices including the entire catheter area and axillary lymph nodes (ALN). For catheter image quantification, to avoid manual bias of surrounding areas, a new VOI was generated semiautomatically using the threshold of 60% of maximum pixel for SUV mean calculation (SUV60 index). Due to the small size of ALN, [^{18}F]FDG uptake was quantified and expressed as the mean of the 5 pixels with the highest uptake (SUVmax) included in the VOI selected (25).

[^{18}F]FDG-MicroPET *in vivo* monitoring of antimicrobial therapy against *S. aureus* ATCC 15981 biofilm infection. Sealed catheters precolonized with *S. aureus* ATCC 15981 were implanted subcutaneously in 20 mice, as described above. From day 1 to day 7, 10 of these mice were treated daily with 0.1 ml of rifampin at 5 mg/ml diluted with PBS (0.5 mg/mouse of Rifaldin; Sanofi-Aventis, France) by the oroesophagical route (Fig. 1D). The remaining 10 mice received PBS and were used as untreated controls. At days 1, 7, and 14 PI, a subgroup of mice ($n = 5$) were arbitrarily selected from both the untreated and the treated groups and monitored by [^{18}F]FDG-MicroPET image analysis (see above). At 7 and 14 days PI, the 5 mice used for MicroPET image were also used for determining the number of CFU/catheter, 24 h after radiotracer administration (when it was completely cleaned from the animal). Moreover, resistance to rifampin was assessed in a pool of recovered colonies, according to the standard MIC microdilution broth method (26).

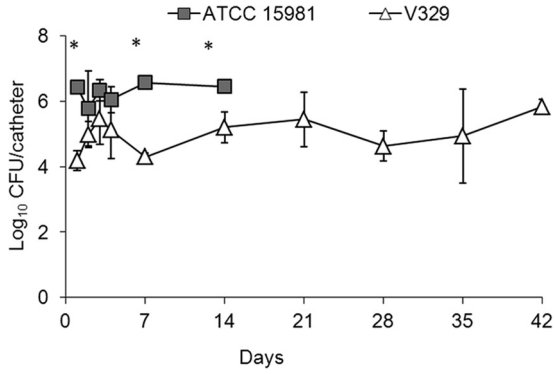

FIG 2 Quantification (mean ± SD; $n = 5$) of viable *S. aureus* ATCC 15981 and V329 bacteria (CFU) found on infected sealed catheters precolonized with the correspondent *S. aureus* strain and implanted subcutaneously in mice. Catheters infected with strain ATCC 15981 (close squares) were naturally expelled between days 7 and 14 postimplantation (PI). At each interval, 1 of 5 catheters successfully precolonized *in vitro* with strain V329 became uninfected after subcutaneous implantation *in vivo*, and the corresponding data have not been included in the figure. Statistical comparisons by Fisher's LSD test showed that *P* values of <0.05 (*) for comparisons between the two bacterial strains were detected at days 1, 7, and 14.

Statistical analysis. The Kolmogorov-Smirnov test was first applied to assess the normal distribution of data. Statistical comparison of means was performed by one-way analysis of variance (ANOVA) (CFU data) or repeated-measures ANOVA (MicroPET data) tests, followed by Fisher's protected least significant difference (PLSD) test. Mathematical and statistical analyses were performed using StatViewGraphics for Windows (SAS Institute Inc.).

RESULTS

Differences between *S. aureus* strains in clinical evaluation, *in vivo* kinetics of bacteria adhered to the surface of catheters, and *in vitro* cytotoxicity. Signs of sepsis or discomfort were not found in any mice throughout the experimental period. Upon palpation, the majority of the animals with infected catheters had local subcutaneous inflammatory reactions on the back by day 7 PI, which were stronger for strain ATCC 15981 than for strain V329. The number of viable bacteria adhered to the surface of sealed catheters was in all cases around 0.8×10^5 CFU at the time of implantation, for both bacterial strains. Thereafter, *S. aureus* ATCC 15981 persisted on catheters at high levels (around 6 log CFU/catheter) up to day 14 PI (Fig. 2), but most (21 of 25) of the devices were naturally expelled before this period. In contrast, all mice with *S. aureus* V329 infection maintained the catheters throughout the experimental period. In these mice, the number of viable V329 bacteria adhered to catheters increased moderately from days 1 to 3 PI, persisting thereafter at stable levels, around 4 to 5 log CFU/catheter (Fig. 2). Systematically, 1 of the 5 mice analyzed per experimental group receiving *S. aureus* V329-precolonized catheters was found free of infection from day 2 to the end of the experiment, indicating a 20% decreased success of catheter infection persistence *in vivo* when using this strain. Comparatively, mice carrying catheters successfully infected by V329 showed lower ($P < 0.05$) bacterial counts per catheter than those infected by ATCC 15981 at any time point (up until day 14 PI, when ATCC 15981-infected catheters were no longer retained subcutaneously).

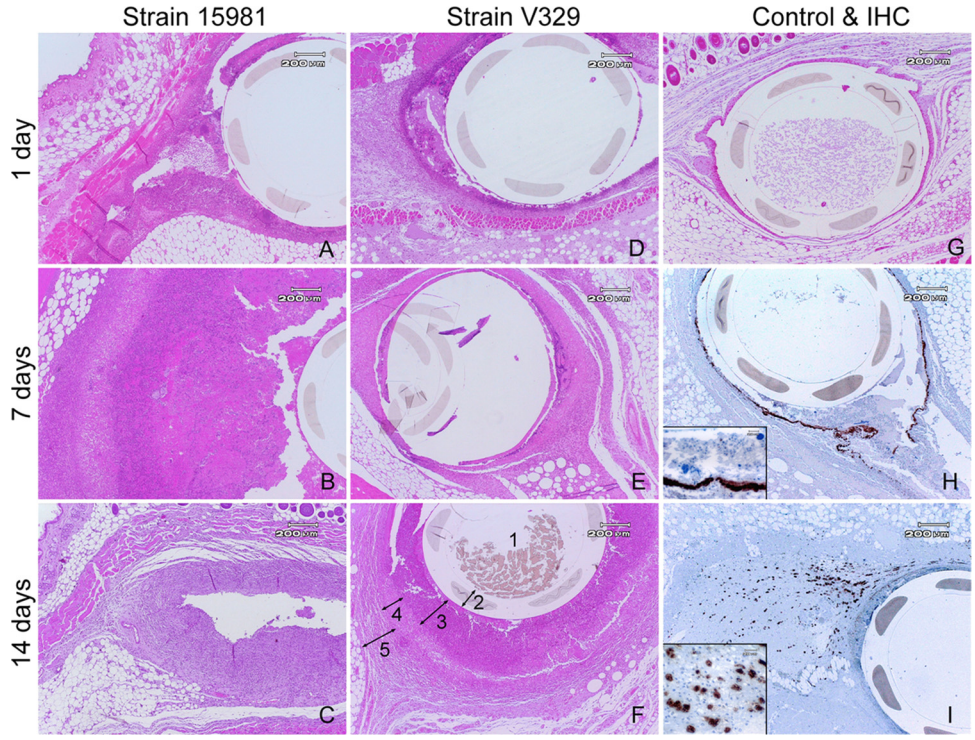

FIG 3 Histological study on *in vivo* biofilm infections in subcutaneous tissues surrounding the catheter, stained with H&E (A to G) or by immunohistochemistry techniques (H and I). Sealed catheters precolonized with *S. aureus* strains ATCC 15981 (A to C) or V329 (D to F) were implanted subcutaneously in mice, and histological analysis was performed on days 1 (A and D), 7 (B and E), and 14 (C and F) PI. At day 14, all mice infected with ATCC 15981 had expelled the catheter (C). Mice carrying uninfected catheters were used as controls (G). IHC allowed the detection of either Bap antigen in *S. aureus* V329 biofilm bacteria (H) or PIA/PNAG antigen in foam cells of *S. aureus* ATCC 15981 disseminated in tissues surrounding the catheter (I). 1, lumen; 2, catheter; 3, cell debris and infiltration of neutrophils; 4, infiltration of macrophages; 5, fibroblasts and connective capsule (F).

On the other hand, the *in vitro* cytotoxicity assay revealed that the ATCC 15981 extract had a higher cytotoxic capacity than that of strain V329. In fact, from the total MDTF viable cells counted by fluorescence-activated cell sorter (FACS) (7,297.7 cellular events counted in the untreated control), reductions of 44.2% (3,225.2 dyed cells) and 5.1% (373.2 dyed cells) were detected when ATCC 15981 and V329 extracts were used, respectively.

Overall, these results indicated the existence of *in vivo* bacterial strain differences regarding the number of live bacteria on the catheter and the capacity of triggering catheter expelling, which could be related to the *in vitro* cytotoxicity of bacterial extracts.

Histopathology and immunohistochemistry. The above observations on infection dynamics and cytotoxicity encouraged the study of inflammatory reactions, under the hypothesis that *S. aureus* ATCC 15981 and V329 infections would differ in the timing (kinetics) and strength of immune/inflammatory reactions. Histological studies revealed that at day 1 PI, uninfected control mice had only a mild diffuse edema and few neutrophils surrounding the catheter area, both disappearing by day 7 PI (Fig. 3). This was compatible with unspecific inflammation subsequent to the surgical implantation of the catheter. In contrast, both bacterial biofilm infections induced prolonged focal and diffuse inflammatory responses, more intense in *S. aureus* ATCC 15981 than in V329 infections (Table 1). The focal reaction triggered by strain ATCC 15981 reached a maximum by day 7 and involved mainly neutrophils, fibroblasts, cell debris, and some macrophages (Table 1 and Fig. 3). The ATCC 15981-triggered reaction strength decreased by day 14 PI as a result of the natural expelling of catheters mentioned above (Table 1). Comparatively, strain V329 induced a delayed focal inflammatory reaction characterized mainly by cell debris (day 7) and macrophages (day 14), with no signs of remission. Overall, these histological findings are in line with the cytotoxicity differences observed *in vitro*, since focal reaction with cell debris and neutrophil infiltration (Table 1 and Fig. 3) could be considered to be partially a result of bacterial cytotoxic effect and, in fact, this effect was earlier and stronger in ATCC 15981 than in V329 infections.

Regarding the mouse connective capsule production, during the first week of infection strain ATCC 15981 induced a thin capsule that disappeared by day 14, accompanied by catheter expelling. In contrast, the capsule induced by strain V329 appeared at day 7 and became moderately thick by day 14 PI (Table 1).

As expected from the nature of the biofilm matrix and the specificity of the anti-matrix-polymer antibodies used, the anti-Bap and anti-PIA/PNAG antibodies stained specifically free bacteria, bacterial aggregates, and neutrophil-phagocytized bacterial antigen in *S. aureus* strain V329 and ATCC 15981 infections, respectively (Fig. 3H and I). Strikingly, anti-PIA/PNAG antibody (and not anti-Bap or control normal rabbit serum) stained the cytoplasm of foam cells disseminated far away from the catheter, between the muscular and adipose tissues in the ATCC 15981 but not in the V329 infection (Fig. 3I). Uninfected animals did not yield positive reactions with anti-PIA/PNAG, anti-Bap antibodies, or control normal rabbit serum.

TABLE 1 Inflammatory reaction observed with hematoxylin and eosin staining after subcutaneous implantation of sealed catheters in mice[a]

Inflammatory reaction	Strength of reaction after catheter colonization with *S. aureus* strain:							
	ATCC 15981			V329			None (uninfected controls)	
	1 DPI	7 DPI	14 DPI[b]	1 DPI	7 DPI	14 DPI	1 DPI	7–14 DPI
Focal	+	+	−	+	+	+	+	+
Cell debris	++	+++	+	++	+++	++	−	−
Neutrophils	+++	++++	+	++	+	++	+	−
Macrophages	+	++	++	−	+	+++	−	−
Fibroblasts	+	+++	++	−	++	++	−	−
Size of capsule	+	+	−	−	+	++	−	−
Diffuse								
Edema	+++	+	−	+++	−	−	+++	−
Neutrophils	+++	++	+	++	+	++	+	−
Macrophages	−	+	−	−	−	+	−	−
Fibroblasts	−	+++	−	−	+++	++	−	−

[a] Symbols: −, absent to very low; +, low; ++, moderate; +++, strong; ++++, very strong. Number of animals/group/assessment day: $n = 5$ for each of the infected groups and $n = 1$ for uninfected controls per time point.
[b] All mice infected with strain ATCC 15981 had expelled the catheters by 14 DPI, and data obtained then refer to these mice that had already lost the implants.

***In vivo* ATCC 15981 and V329 infections monitoring by MicroPET.** Knowing the above strain differences, we examined whether the two *S. aureus* infections could be assessed and would differ *in vivo* by MicroPET imaging analysis, according to the experiment outlined in Fig. 1C. Unlike what was observed in uninfected controls, [^{18}F]FDG was increased in both catheter and ALN areas of infected mice (Fig. 4).

In the catheter area (Fig. 4A and C, left panel), [^{18}F]FDG uptake was detected as soon as day 1 PI and remained stable for each bacterial strain, without statistical differences in the mean SUV60 index values for a given strain along the study period. In addition, strain differences were detected by increased ($P < 0.05$) SUV60 values in ATCC 15981 compared to V329 infections on days 7 and 14 PI.

In ALN (Fig. 4B and C, right panel), SUVmax values were very low or null at day 1 PI, increasing significantly by day 7 PI in ATCC 15981 infections but only moderately and with a delay (i.e., by day 14 PI) in V329 infections. Thus, differences between day 1 and days 7 or 14 PI were highly significant ($P \leq 0.0005$) in ATCC 15981 infection, but they were only a trend ($P = 0.08$) in *S. aureus* V329 infection. Overall, [^{18}F]FDG uptake was detected in the catheter area earlier than in ALN, but in ALN the signal remained at high levels after catheter expelling, as presented in Fig. 4B.

Altogether, these results indicated that the early (day 7) and strong [^{18}F]FDG uptake observed in ATCC 15981 infection (Fig. 4) corresponded to an early and strong inflammatory reaction (Fig. 3) and increased cytotoxicity triggered by this strain compared to strain V329. Also, in V329-infected mice, the steady increase in ALN SUVmax index corresponded to the steady increase in focal subcutaneous inflammatory reaction (Fig. 3).

[^{18}F]FDG-MicroPET image analysis for evaluating the effect of a rifampin treatment. The strong and stable [^{18}F]FDG uptake in *S. aureus* ATCC 15981 infections suggested that this strain was a good choice as a prototype to determine the utility of the [^{18}F]FDG-MicroPET mouse model for monitoring *in vivo* the effect of an antibiotic treatment with rifampin as a standard drug against *S. aureus* (Fig. 1D). As shown in Fig. 5, the SUV60 and SUVmax values obtained in the untreated group were very close to those obtained in the previous experiment (Fig. 4), indicating the repeatability of the method. The SUV60 values in the catheter area (Fig. 5A and B, left panels) decreased significantly ($P < 0.05$) by day 7 in the rifampin-treated group. This decrease was accompanied by a significant ($P < 0.005$) decrease at day 7 in the number of CFU/catheter (Fig. 5C). Also, treated animals maintained the catheter beyond day 14, this being a sign of controlled infection. However, an increase ($P < 0.05$) in the SUV60 index was observed at an individual level in some rifampin-treated animals by day 14 PI compared to day 7 (Fig. 5A, left panel). This fluctuation of SUV60 values was likely due to the appearance of rifampin-resistant variants of *S. aureus* ATCC 15981, as verified by the MIC assay (16 μg/ml for recovered colonies versus 0.025 μg/ml for the reference strain). Finally, the SUVmax values in ALN of rifampin-treated mice were null until day 7 (Fig. 5A and B, right panels) and increased slightly at day 14 PI (Fig. 5A, right panel).

DISCUSSION

The utility of an innovative [^{18}F]FDG-MicroPET *in vivo* imaging technology in *S. aureus* biofilm infections was assessed in a sealed-catheter mouse model developed in this work. This mouse model was found useful for (i) monitoring long-term *S. aureus in vivo* infections in the same animal, (ii) detecting *S. aureus* strain differences in infection dynamics and pathogenicity, and (iii) evaluating the effect of antimicrobial therapy using unlabeled bacteria.

To our knowledge, this is the first work using the [^{18}F]FDG-MicroPET image method for diagnosing and monitoring bacterial biofilm evolution in mice. This method has been successfully applied for diagnosing clinical inflammatory processes, especially those involving neutrophils and macrophages (27, 28). However, bacteria may also take up [^{18}F]FDG *in vivo*, since PIA/PNAG-dependent *S. aureus* biofilm production *in vitro* may be enhanced by glucose supplementation (TSB-glc here). Unfortunately, the technique did not distinguish the signal emitted exclusively by bacteria from that generated by inflammatory cells. [^{18}F]FDG-MicroPET has also been used in animals, specifically in rabbit staphylococcal osteomyelitis models (18, 19). The mouse model, which involved the use of sealed catheters and required a one-step

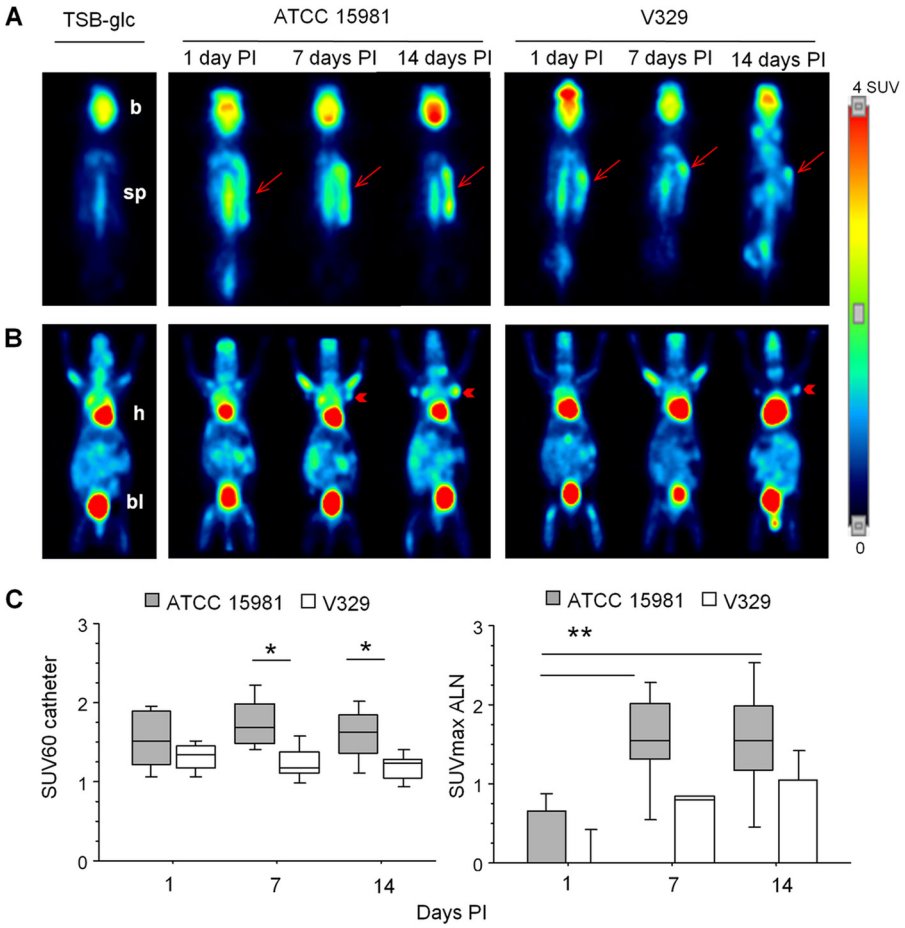

FIG 4 Representative [^{18}F]FDG-MicroPET images in mice carrying catheters infected with *S. aureus* strains ATCC 15981 or V329. Slices at dorsal (A) and ventral (B) positions show [^{18}F]-FGD uptake in catheter (arrows) or axillary lymph node (ALN; arrowheads) areas, respectively. Brain (b), heart (h), bladder (bl), and spinal cord (sp) show physiological uptake of [^{18}F]-FGD. In panels A and B, each image corresponds to a representative animal analyzed at days 1, 7, and 14 PI. Images of uninfected controls (receiving only TSB-glc) are included on the left. (C) Box plots illustrating the evolution of the SUV60 index in *S. aureus* ATCC 15981 or V329 infections in the catheter area (left panel) and SUVmax in ALN (right panel). Statistical comparisons by Fisher's PLSD test: *, $P < 0.05$; **, $P < 0.005$.

rather than a two-step (10, 11) surgical procedure in the absence of a cement block, simplified the assessment of direct host-pathogen interactions. In line with our observations, in a rabbit model detecting bone staphylococcal infections, a direct relationship was found between PET image intensity, degree of leukocyte infiltration, and increased virulence (in *S. aureus* compared to *S. epidermidis*) (18). However, detection of *S. aureus* strain differences and antibiotic monitoring was not attempted.

Both *S. aureus* strains involved in our study were strong biofilm producers to guarantee a successful catheter precolonization and subsequently attempt chronic infection in mice. The SUV image differences detected *in vivo* between bacterial strains were in consonance not only with those found in infection kinetics and cytotoxicity differences but also with strain-associated differences in bacterial dissemination and the triggered histological changes. The strain differences in the *in vivo* colonization capacity may be attributed to the defective primary binding of V329 Bap-synthesizing bacteria via host molecules (29, 30) and to the tight cell-to-cell Bap-mediated bonds compared to PIA/PNAG-mediated binding (ATCC 15981 biofilms). The decreased inflammatory reaction triggered by V329 compared to ATCC 15981 can be explained by the decreased number of bacteria adhered to the catheters *in vivo*, the diminished cytotoxicity *in vitro*, and the natural replacement of toxin genes by the *bap* gene in strain V329 (1, 23). In contrast, the intense inflammatory reaction triggered by ATCC 15981 was expected, as this clinical otitis isolate, which encodes exocellular proteases (21), had a high colonization capacity and was highly cytotoxic, all of which may have triggered the expulsion of infected catheters.

The finding that the [^{18}F]FDG-MicroPET uptake in untreated mice was delayed in the draining ALN compared to the catheter area was compatible with the development of an adaptive immune response in the ALN within a 2-week period following the immune response at the initial infection site. This is in agreement with a previous study evaluating *S. aureus*-contaminated muscle injury in rabbits through histological and microbiological analysis (31), in which the draining lymph node provided a delayed signal compared to that of the originally infected body site. Altogether, these observations outline the utility of draining lymph node [^{18}F]FDG-MicroPET imaging in chronic infections.

Biofilm-embedded bacteria are tenacious and 100 to 10,000 times more resistant to antimicrobial treatment than nonembed-

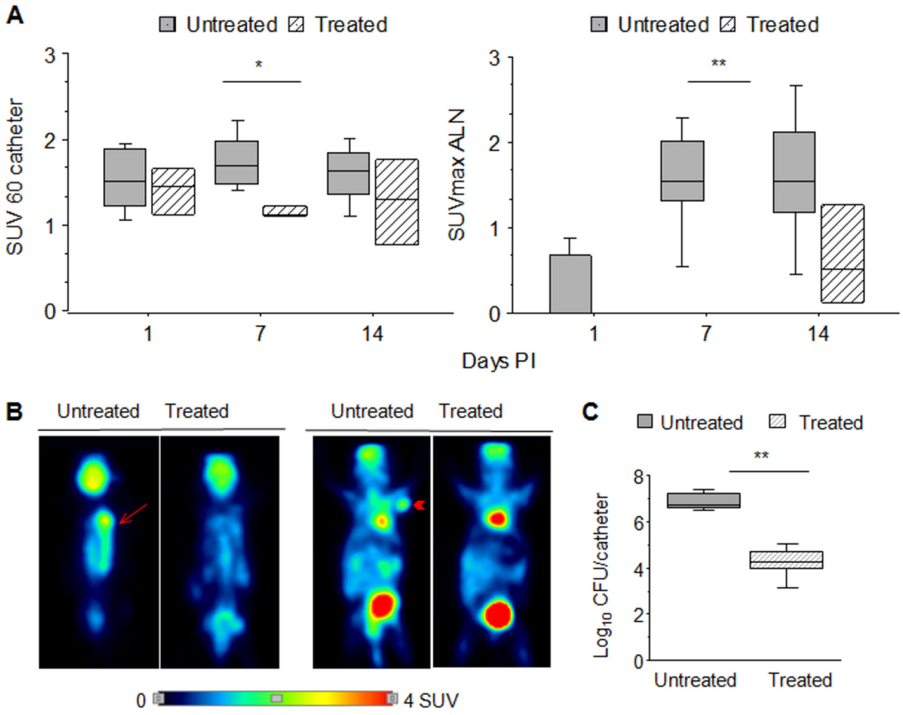

FIG 5 Evaluation of rifampin treatment effect using [^{18}F]FDG-MicroPET imaging in mice carrying sealed catheters precolonized with *S. aureus* strain ATCC 15981. (A) Box plot representation of [^{18}F]FDG-MicroPET uptake quantification at days 1, 7, and 14 postimplantation (PI) in catheter (left panel) or ALN (right panel) areas of mice, either untreated (dark boxes) or rifampin treated (striped light boxes). (B) MicroPET images of representative untreated and treated mice, in dorsal (left images) or ventral (right images) positions showing the catheter area (arrow) and ALN (arrowheads), respectively. (C) Box plots representing the number of bacteria (log CFU/catheter) adhered to the surface of sealed catheters in untreated (dark boxes) and rifampin-treated (striped light boxes) mice. Asterisks represent differences between groups, when they became more evident and statistically significant (*, $P < 0.05$; **, $P < 0.005$ by Fisher's PLSD test).

ded bacteria, even *in vitro* (32, 33). Different studies show that treatment with high doses of rifampin is effective against *S. aureus* biofilm bacteria *in vitro* (33–35) and *in vivo* (12), but it leads also to the appearance of rifampin-resistant variants carrying mutations in the *rpoB* gene and consequently to increased bacterial counts and optical imaging signal, as observed in studies on natural human device infections (36) and mouse intravenous catheter infections using *lux*-labeled bacteria (10, 13). Thus, the appearance of resistant variants, verified *in vitro*, was not only expected but also advantageous in our model since it allowed the detection of variation in [^{18}F]FDG-MicroPET uptake intensity through the duration of the treatment. Finally, the absence of catheter expelling and of PET image signal in ALN upon antibiotic treatment could be considered indicative of antibiotic efficacy and points out the value of ALN to assess immune response and infection progress in the model applied.

The [^{18}F]FDG-MicroPET mouse model allowed follow-up individual studies, reducing the number of euthanized experimental animals, in line with the current international guidelines on animal welfare. A promising near-infrared fluorescence imaging mouse model using an alternative precolonized device (polymer disk) to detect inflammation (reactive oxygen species produced by inflammatory cells) upon implantation has been developed recently (14). The utility of this model to assess differences in pathogenicity between bacterial strains and to monitor the effect of antibiotic therapy has not been reported so far.

Overall, the model was highly reproducible, with a low intragroup or interexperiment variability; of note, the *in vivo* follow-up studies using individually identified animals allowed an individual evaluation of the infection. Also, the model and technology applied involve decreased attendant costs and manual laboratory work, by minimizing the number of animals used, and could be suitable for preclinical studies, as it could yield useful data to diagnose *S. aureus* biofilm infections and to develop, improve, and monitor single and combined antimicrobial treatments. Finally, the model could be successfully employed to assess *in vivo* differences between natural isolates and/or genetically modified bacteria in virulence/pathogenicity and to investigate host-pathogen interactions of clinical relevance in device-associated and biofilm infections.

ACKNOWLEDGMENTS

This work was supported by grants from Gobierno de Navarra "IIM13002.RI1" and MICINN "CIT-010000-2009-32."

We thank Ramsés Reina (Instituto de Agrobiotecnología, Pamplona, Spain) for cell culture, Gerry Pier (Harvard Medical School, USA) for anti-PIA/PNAG antibody, and I. Lasa and his group (Instituto de Agrobiotecnología, Pamplona, Spain) for anti-Bap antibody and support on technical approaches.

REFERENCES

1. **Cucarella C, Solano C, Valle J, Amorena B, Lasa I, Penades JR.** 2001. Bap, a *Staphylococcus aureus* surface protein involved in biofilm formation. J. Bacteriol. **183:**2888–2896. http://dx.doi.org/10.1128/JB.183.9.2888-2896.2001.
2. **Valle J, Vergara-Irigaray M, Merino N, Penades JR, Lasa I.** 2007. Sigma^{B} regulates IS256-mediated *Staphylococcus aureus* biofilm phenotypic variation. J. Bacteriol. **189:**2886–2896. http://dx.doi.org/10.1128/JB.01767-06.

3. **Heilmann C, Gerke C, Perdreau-Remington F, Gotz F.** 1996. Characterization of Tn917 insertion mutants of *Staphylococcus epidermidis* affected in biofilm formation. Infect. Immun. **64:**277–282.
4. **Cramton SE, Gerke C, Schnell NF, Nichols WW, Gotz F.** 1999. The intercellular adhesion (ica) locus is present in *Staphylococcus aureus* and is required for biofilm formation. Infect. Immun. **67:**5427–5433.
5. **McKenney D, Pouliot KL, Wang Y, Murthy V, Ulrich M, Doring G, Lee JC, Goldmann DA, Pier GB.** 1999. Broadly protective vaccine for *Staphylococcus aureus* based on an *in vivo*-expressed antigen. Science **284:**1523–1527. http://dx.doi.org/10.1126/science.284.5419.1523.
6. **Vergara-Irigaray M, Valle J, Merino N, Latasa C, Garcia B, Ruiz de Los Mozos I, Solano C, Toledo-Arana A, Penades JR, Lasa I.** 2009. Relevant role of fibronectin-binding proteins in *Staphylococcus aureus* biofilm-associated foreign-body infections. Infect. Immun. **77:**3978–3991. http://dx.doi.org/10.1128/IAI.00616-09.
7. **Christner M, Franke GC, Schommer NN, Wendt U, Wegert K, Pehle P, Kroll G, Schulze C, Buck F, Mack D, Aepfelbacher M, Rohde H.** 2010. The giant extracellular matrix-binding protein of *Staphylococcus epidermidis* mediates biofilm accumulation and attachment to fibronectin. Mol. Microbiol. **75:**187–207. http://dx.doi.org/10.1111/j.1365-2958.2009.06981.x.
8. **Pozzi C, Waters EM, Rudkin JK, Schaeffer CR, Lohan AJ, Tong P, Loftus BJ, Pier GB, Fey PD, Massey RC, O'Gara JP.** 2012. Methicillin resistance alters the biofilm phenotype and attenuates virulence in *Staphylococcus aureus* device-associated infections. PLoS Pathog. **8:**e1002626. http://dx.doi.org/10.1371/journal.ppat.1002626.
9. **Laverty G, Gorman SP, Gilmore BF.** 2013. Biomolecular mechanisms of staphylococcal biofilm formation. Future Microbiol. **8:**509–524. http://dx.doi.org/10.2217/fmb.13.7.
10. **Kadurugamuwa JL, Sin L, Albert E, Yu J, Francis K, DeBoer M, Rubin M, Bellinger-Kawahara C, Parr TR, Jr, Contag PR.** 2003. Direct continuous method for monitoring biofilm infection in a mouse model. Infect. Immun. **71:**882–890. http://dx.doi.org/10.1128/IAI.71.2.882-890.2003.
11. **Merino N, Toledo-Arana A, Vergara-Irigaray M, Valle J, Solano C, Calvo E, Lopez JA, Foster TJ, Penades JR, Lasa I.** 2009. Protein A-mediated multicellular behavior in *Staphylococcus aureus*. J. Bacteriol. **191:**832–843. http://dx.doi.org/10.1128/JB.01222-08.
12. **Kadurugamuwa JL, Sin LV, Yu J, Francis KP, Kimura R, Purchio T, Contag PR.** 2003. Rapid direct method for monitoring antibiotics in a mouse model of bacterial biofilm infection. Antimicrob. Agents Chemother. **47:**3130–3137. http://dx.doi.org/10.1128/AAC.47.10.3130-3137.2003.
13. **Kadurugamuwa JL, Sin LV, Yu J, Francis KP, Purchio TF, Contag PR.** 2004. Noninvasive optical imaging method to evaluate postantibiotic effects on biofilm infection *in vivo*. Antimicrob. Agents Chemother. **48:**2283–2287. http://dx.doi.org/10.1128/AAC.48.6.2283-2287.2004.
14. **Dinjaski N, Suri S, Valle J, Lehman SM, Lasa I, Prieto MA, Garcia AJ.** 2014. Near-infrared fluorescence imaging as an alternative to bioluminescent bacteria to monitor biomaterial-associated infections. Acta Biomater. **10:**2935–2944. http://dx.doi.org/10.1016/j.actbio.2014.03.005.
15. **Israel O, Keidar Z.** 2011. PET/CT imaging in infectious conditions. Ann. N. Y. Acad. Sci. **1228:**150–166. http://dx.doi.org/10.1111/j.1749-6632.2011.06026.x.
16. **Jamar F, Buscombe J, Chiti A, Christian PE, Delbeke D, Donohoe KJ, Israel O, Martin-Comin J, Signore A.** 2013. EANM/SNMMI guideline for 18F-FDG use in inflammation and infection. J. Nucl. Med. **54:**647–658. http://dx.doi.org/10.2967/jnumed.112.112524.
17. **Catana C, Procissi D, Wu Y, Judenhofer MS, Qi J, Pichler BJ, Jacobs RE, Cherry SR.** 2008. Simultaneous *in vivo* positron emission tomography and magnetic resonance imaging. Proc. Natl. Acad. Sci. U. S. A. **105:**3705–3710. http://dx.doi.org/10.1073/pnas.0711622105.
18. **Lankinen P, Lehtimaki K, Hakanen AJ, Roivainen A, Aro HT.** 2012. A comparative ^{18}F-FDG PET/CT imaging of experimental *Staphylococcus aureus* osteomyelitis and *Staphylococcus epidermidis* foreign-body-associated infection in the rabbit tibia. EJNMMI Res. **2:**41. http://dx.doi.org/10.1186/2191-219X-2-41.
19. **Koort JK, Makinen TJ, Knuuti J, Jalava J, Aro HT.** 2004. Comparative ^{18}F-FDG PET of experimental *Staphylococcus aureus* osteomyelitis and normal bone healing. J. Nucl. Med. **45:**1406–1411.
20. **Toledo-Arana A, Merino N, Vergara-Irigaray M, Debarbouille M, Penades JR, Lasa I.** 2005. *Staphylococcus aureus* develops an alternative, ica-independent biofilm in the absence of the arlRS two-component system. J. Bacteriol. **187:**5318–5329. http://dx.doi.org/10.1128/JB.187.15.5318-5329.2005.
21. **Valle J, Toledo-Arana A, Berasain C, Ghigo JM, Amorena B, Penades JR, Lasa I.** 2003. SarA and not sigma^B is essential for biofilm development by *Staphylococcus aureus*. Mol. Microbiol. **48:**1075–1087. http://dx.doi.org/10.1046/j.1365-2958.2003.03493.x.
22. **Tormo MA, Ubeda C, Marti M, Maiques E, Cucarella C, Valle J, Foster TJ, Lasa I, Penades JR.** 2007. Phase-variable expression of the biofilm-associated protein (Bap) in *Staphylococcus aureus*. Microbiology **153:**1702–1710. http://dx.doi.org/10.1099/mic.0.2006/005744-0.
23. **Cucarella C, Tormo MA, Ubeda C, Trotonda MP, Monzon M, Peris C, Amorena B, Lasa I, Penades JR.** 2004. Role of biofilm-associated protein bap in the pathogenesis of bovine *Staphylococcus aureus*. Infect. Immun. **72:**2177–2185. http://dx.doi.org/10.1128/IAI.72.4.2177-2185.2004.
24. **Amorena B, García de Jalón JA, Baselga R, Ducha J, Latre MV, Ferrer LM, Sancho F, Mansson I, Krovacek Faris KA.** 1991. Experimental infection in mammary glands with ovine mastitis bacterial strains: evaluation of a rabbit model. J. Comp. Pathol. **104:**289–302. http://dx.doi.org/10.1016/S0021-9975(08)80041-2.
25. **Straver ME, Aukema TS, Olmos RA, Rutgers EJ, Gilhuijs KG, Schot ME, Vogel WV, Peeters MJ.** 2010. Feasibility of FDG PET/CT to monitor the response of axillary lymph node metastases to neoadjuvant chemotherapy in breast cancer patients. Eur. J. Nucl. Med. Mol. Imaging **37:**1069–1076. http://dx.doi.org/10.1007/s00259-009-1343-2.
26. **Murray PR, Baron EJ, Jorgensen JH, Phaller MA, Yolken RH.** 2003. Manual of clinical microbiology, 8th ed. ASM, Press, Washington, DC.
27. **Gamelli RL, Liu H, He LK, Hofmann CA.** 1996. Augmentations of glucose uptake and glucose transporter-1 in macrophages following thermal injury and sepsis in mice. J. Leukoc. Biol. **59:**639–647.
28. **Mochizuki T, Tsukamoto E, Kuge Y, Kanegae K, Zhao S, Hikosaka K, Hosokawa M, Kohanawa M, Tamaki N.** 2001. FDG uptake and glucose transporter subtype expressions in experimental tumor and inflammation models. J. Nucl. Med. **42:**1551–1555.
29. **Cucarella C, Tormo MA, Knecht E, Amorena B, Lasa I, Foster TJ, Penades JR.** 2002. Expression of the biofilm-associated protein interferes with host protein receptors of *Staphylococcus aureus* and alters the infective process. Infect. Immun. **70:**3180–3186. http://dx.doi.org/10.1128/IAI.70.6.3180-3186.2002.
30. **Valle J, Latasa C, Gil C, Toledo-Arana A, Solano C, Penades JR, Lasa I.** 2012. Bap, a biofilm matrix protein of *Staphylococcus aureus* prevents cellular internalization through binding to GP96 host receptor. PLoS Pathog. **8:**e1002843. http://dx.doi.org/10.1371/journal.ppat.1002843.
31. **Eardley WG, Martin KR, Taylor C, Kirkman E, Clasper JC, Watts SA.** 2012. The development of an experimental model of contaminated muscle injury in rabbits. Int. J. Low. Extrem. Wounds **11:**254–263.
32. **Monzon M, Oteiza C, Leiva J, Lamata M, Amorena B.** 2002. Biofilm testing of *Staphylococcus* epidermidis clinical isolates: low performance of vancomycin in relation to other antibiotics. Diagn. Microbiol. Infect. Dis. **44:**319–324. http://dx.doi.org/10.1016/S0732-8893(02)00464-9.
33. **Amorena B, Gracia E, Monzon M, Leiva J, Oteiza C, Perez M, Alabart JL, Hernandez-Yago J.** 1999. Antibiotic susceptibility assay for *Staphylococcus aureus* in biofilms developed *in vitro*. J. Antimicrob. Chemother. **44:**43–55. http://dx.doi.org/10.1093/jac/44.1.43.
34. **Saginur R, Stdenis M, Ferris W, Aaron SD, Chan F, Lee C, Ramotar K.** 2006. Multiple combination bactericidal testing of staphylococcal biofilms from implant-associated infections. Antimicrob. Agents Chemother. **50:**55–61. http://dx.doi.org/10.1128/AAC.50.1.55-61.2006.
35. **El Helou OC, Berbari EF, Lahr BD, Eckel-Passow JE, Razonable RR, Sia IG, Virk A, Walker RC, Steckelberg JM, Wilson WR, Hanssen AD, Osmon DR.** 2010. Efficacy and safety of rifampin containing regimen for staphylococcal prosthetic joint infections treated with debridement and retention. Eur. J. Clin. Microbiol. Infect. Dis. **29:**961–967. http://dx.doi.org/10.1007/s10096-010-0952-9.
36. **Achermann Y, Eigenmann K, Ledergerber B, Derksen L, Rafeiner P, Clauss M, Nuesch R, Zellweger C, Vogt M, Zimmerli W.** 2013. Factors associated with rifampin resistance in staphylococcal periprosthetic joint infections (PJI): a matched case-control study. Infection **41:**431–437. http://dx.doi.org/10.1007/s15010-012-0325-7.